




CYLD is a causative gene for frontotemporal dementia – amyotrophic lateral sclerosis

Carol Dobson-Stone,^{1,2,3} Marianne Hallupp,^{1,2} Hamideh Shahheydari,⁴
 Audrey M.G. Ragagnin,⁴ Zac Chatterton,^{1,5,6} Francine Carew-Jones,^{2,3}
 Claire E. Shepherd,^{2,3} Holly Stafen,⁷ Esmeralda Paric,⁷ Thomas Fath,⁷
 Elizabeth M. Thompson,^{8,9} Peter Blumbergs,¹⁰ Cathy L. Short,¹¹ Colin D. Field,¹²
 Peter K. Panegyres,¹³ Jane Hecker,¹⁴ Garth Nicholson,^{15,16,17} Alex D. Shaw,^{1,2,3}
 Janice M. Fullerton,^{2,3} Agnes A. Luty,^{2,3} Peter R. Schofield,^{2,3} William S. Brooks,^{2,18}
 Neil Rajan,¹⁹  Mark F. Bennett,^{20,21,22} Melanie Bahlo,^{20,22}  Shankaracharya,²³
 John E. Landers,²³ Olivier Piguet,^{24,25} John R. Hodges,^{1,25}  Glenda M. Halliday,^{1,2,3}
 Simon D. Topp,²⁶ Bradley N. Smith,²⁶ Christopher E. Shaw,²⁶ Emily McCann,⁴
 Jennifer A. Fifita,⁴ Kelly L. Williams,⁴ Julie D. Atkin,^{4,27} Ian P. Blair⁴ and John B. Kwok^{1,2,3}

Frontotemporal dementia and amyotrophic lateral sclerosis are clinically and pathologically overlapping disorders with shared genetic causes. We previously identified a disease locus on chromosome 16p12.1-q12.2 with genome-wide significant linkage in a large European Australian family with autosomal dominant inheritance of frontotemporal dementia and amyotrophic lateral sclerosis and no mutation in known amyotrophic lateral sclerosis or dementia genes. Here we demonstrate the segregation of a novel missense variant in *CYLD* (c.2155A>G, p.M719V) within the linkage region as the genetic cause of disease in this family. Immunohistochemical analysis of brain tissue from two *CYLD* p.M719V mutation carriers showed widespread glial *CYLD* immunoreactivity. Primary mouse neurons transfected with *CYLD*_{M719V} exhibited increased cytoplasmic localization of TDP-43 and shortened axons. *CYLD* encodes a lysine 63 deubiquitinase and *CYLD* cutaneous syndrome, a skin tumour disorder, is caused by mutations that lead to reduced deubiquitinase activity. In contrast with *CYLD* cutaneous syndrome-causative mutations, *CYLD*_{M719V} exhibited significantly increased lysine 63 deubiquitinase activity relative to the wild-type enzyme (paired Wilcoxon signed-rank test $P = 0.005$). Overexpression of *CYLD*_{M719V} in HEK293 cells led to more potent inhibition of the cell signalling molecule NF- κ B and impairment of autophagosome fusion to lysosomes, a key process in autophagy. Although *CYLD* mutations appear to be rare, *CYLD*'s interaction with at least three other proteins encoded by frontotemporal dementia and/or amyotrophic lateral sclerosis genes (*TBK1*, *OPTN* and *SQSTM1*) suggests that it may play a central role in the pathogenesis of these disorders. Mutations in several frontotemporal dementia and amyotrophic lateral sclerosis genes, including *TBK1*, *OPTN* and *SQSTM1*, result in a loss of autophagy function. We show here that increased *CYLD* activity also reduces autophagy function, highlighting the importance of autophagy regulation in the pathogenesis of frontotemporal dementia and amyotrophic lateral sclerosis.

- 1 The University of Sydney, Brain and Mind Centre and Central Clinical School, Faculty of Medicine and Health, Camperdown, NSW 2006, Australia
- 2 Neuroscience Research Australia, Randwick, NSW 2031, Australia
- 3 School of Medical Sciences, University of New South Wales, Sydney, NSW 2052, Australia
- 4 Centre for Motor Neuron Disease Research, Department of Biomedical Sciences, Faculty of Medicine and Health Sciences, Macquarie University, North Ryde, NSW 2109, Australia
- 5 Friedman Brain Institute, Icahn School of Medicine at Mount Sinai, New York, NY 10029 USA
- 6 Department of Neuroscience, Icahn School of Medicine at Mount Sinai, New York, NY 10029 USA

Received August 1, 2019. Revised December 1, 2019. Accepted December 17, 2019

© The Author(s) (2020). Published by Oxford University Press on behalf of the Guarantors of Brain. All rights reserved.

For permissions, please email: journals.permissions@oup.com

- 7 Dementia Research Centre and Department of Biomedical Sciences, Faculty of Medicine and Health Sciences, Macquarie University, North Ryde, NSW 2109, Australia
- 8 SA Clinical Genetics Service, Women's and Children's Hospital, North Adelaide 5006, SA, Australia
- 9 Adelaide Medical School, Faculty of Health Sciences, University of Adelaide, Adelaide SA 5005, Australia
- 10 Institute of Medical and Veterinary Science, Adelaide, SA 5000, Australia
- 11 Department of Neurology, The Queen Elizabeth Hospital, Woodville, SA 5011, Australia
- 12 Adelaide Dementia Driving Clinic, Adelaide, SA 5041, Australia
- 13 Neurodegenerative Disorders Research Pty Ltd, West Perth, WA 6005, Australia
- 14 Department of General Medicine, Royal Adelaide Hospital, Adelaide, SA 5000, Australia
- 15 Northcott Neuroscience Laboratory, ANZAC Research Institute, Concord, NSW 2137, Australia
- 16 Sydney Medical School, University of Sydney, Camperdown, NSW 2050, Australia
- 17 Molecular Medicine Laboratory, Concord Hospital, Concord, NSW 2137, Australia
- 18 Prince of Wales Clinical School, University of New South Wales, Sydney, NSW 2052, Australia
- 19 Institute of Genetic Medicine, Newcastle University, Newcastle upon Tyne, NE1 3BZ, UK
- 20 Population Health and Immunity Division, Walter and Eliza Hall Institute of Medical Research, Parkville, VIC 3052, Australia
- 21 Epilepsy Research Centre, Department of Medicine, The University of Melbourne, Austin Health, Heidelberg, VIC 3084, Australia
- 22 Department of Medical Biology, The University of Melbourne, Parkville, VIC 3052, Australia
- 23 University of Massachusetts Medical School, Worcester, MA 01655, USA
- 24 The University of Sydney, Brain and Mind Centre and School of Psychology, Camperdown, NSW 2006, Australia
- 25 ARC Centre of Excellence in Cognition and its Disorders, Sydney, NSW, Australia
- 26 UK Dementia Research Institute, Department of Basic and Clinical Neuroscience, Institute of Psychiatry, Psychology and Neuroscience, Maurice Wohl Clinical Neuroscience Institute, King's College London, London SE5 9RX, UK
- 27 Department of Biochemistry and Genetics, La Trobe Institute for Molecular Science, Bundoora, VIC 3083, Australia

Correspondence to: John B. Kwok
Brain and Mind Centre, University of Sydney, 94 Mallett St, Camperdown, NSW 2050,
Australia
E-mail: john.kwok@sydney.edu.au

Correspondence may also be addressed to: Carol Dobson-Stone
E-mail: carol.dobson-stone@sydney.edu.au

Keywords: genome-wide linkage analysis; whole-exome sequencing; CYLD; deubiquitinase; autophagy

Abbreviations: ALS = amyotrophic lateral sclerosis; CBD = corticobasal degeneration; GFP = green fluorescent protein; FTD = frontotemporal dementia; FTLD = frontotemporal lobar degeneration; LC3 = microtubule associated protein 1 light chain 3; NF- κ B = nuclear factor kappa B; TDP-43 = TAR DNA binding protein 43 kDa

Introduction

Frontotemporal dementia (FTD) is the second most common cause of younger-onset (<65 years old) dementia after Alzheimer's disease (Ratnavalli *et al.*, 2002). FTD is a heterogeneous disorder characterized by personality and behavioural changes, and/or progressive deficits in language expression and comprehension (Seelaar *et al.*, 2011). Around 15% of individuals diagnosed with FTD also develop amyotrophic lateral sclerosis (ALS), a progressive degeneration of upper and lower motor neurons that leads to paralysis and ultimately death (Lillo and Hodges, 2009).

Approximately 40% of FTD cases have an affected relative, suggesting a genetic cause (Goldman *et al.*, 2005). Mutations in several genes have been identified as causes of familial FTD. *MAPT* and *GRN* mutations together account for 10–40% of familial FTD cases (Hutton *et al.*, 1998; Baker *et al.*, 2006; Pottier *et al.*, 2016), and a hexanucleotide repeat expansion in *C9orf72* is the most common genetic cause of familial FTD and ALS (~12% and 24% of familial FTD and familial ALS cases, respectively) (DeJesus-

Hernandez *et al.*, 2011; Renton *et al.*, 2011). Several other genes have been identified as rarer causes of both FTD and ALS, including *VCP*, *OPTN*, *SQSTM1*, *TBK1*, *CCNF* and *TIA1* (Watts *et al.*, 2004; Maruyama *et al.*, 2010; Fecto *et al.*, 2011; Freischmidt *et al.*, 2015; Williams *et al.*, 2016; Mackenzie *et al.*, 2017). Several of these genes have been functionally implicated in autophagy, a process by which the cell removes aggregated or misfolded proteins and damaged organelles (reviewed in Deng *et al.*, 2017; Evans and Holzbaur, 2019). Both optineurin (*OPTN*) and *SQSTM1* (p62) are autophagy receptors that are recruited to ubiquitinated substrates and bind the autophagosome protein LC3 (microtubule associated protein 1 light chain 3, encoded by *MAP1LC3A*) to induce engulfment (Lamark *et al.*, 2017; Markovinic *et al.*, 2017). In addition, TANK binding kinase 1 (*TBK1*) is known to phosphorylate and activate both p62 and *OPTN* (Wild *et al.*, 2011; Pilli *et al.*, 2012).

The aim of this study was to determine the causative mutation in a large European Australian family with FTD-ALS, with no mutations in known dementia or ALS genes. Our previous work provided genome-wide significant evidence of

a disease locus on chromosome 16p12.1-16q12.2 [maximum multipoint logarithm of odds (LOD) score of 3.0], with a maximal critical region of ~38 Mb (GRCh37/hg19 chr16:17473796–55359315) and a smaller suggestive disease haplotype, defined by recombination in an elderly unaffected individual, of ~24 Mb (chr16:31273792–55359315) (Dobson-Stone *et al.*, 2013). Using a comprehensive strategy combining genetic linkage analysis, DNA sequencing, brain immunohistochemical analysis, enzymatic assay and cell culture analyses of axonal morphology, TAR DNA binding protein 43 kDa (TDP-43) localization, nuclear factor kappa B (NF- κ B) activity and autophagic flux, we provide evidence that CYLD lysine 63 deubiquitinase (CYLD; NCBI Gene 1540) at chromosome 16q12.1 is a causal gene for FTD-ALS.

Materials and methods

Subject information

One FTD-ALS family (Family Aus-12, Fig. 1) and four FTD and/or ALS patient cohorts were included in this study. Clinical notes for Family Aus-12 pedigree members have been published previously (Dobson-Stone *et al.*, 2013). Cohort sizes were determined by availability of DNA samples and/or whole-exome sequencing data.

Cohort 1 comprised 132 European ancestry Australian individuals with younger-onset (age <65 years) dementia (51 with family history of younger-onset dementia) recruited or referred for DNA studies of dementia since 1994, via specialist dementia clinics, neurologists, psychiatrists, geriatricians or genetic clinics. Subjects were negative for mutations in *MAPT* and *GRN* and repeat expansions in *C9orf72*.

Cohort 2 comprised 91 European Australian individuals (18 with ≤ 1 relative with neurologist/geriatrician-confirmed FTD or younger-onset dementia or ALS) who had undergone precise clinical phenotyping at FRONTIER, an FTD research clinic in Sydney (28 behavioural variant FTD, 23 semantic dementia, 14 progressive non-fluent aphasia, two progressive supranuclear palsy, seven corticobasal syndrome and 17 FTD-ALS). Patients were negative for mutations in *MAPT* and *GRN* and repeat expansions in *C9orf72*.

Cohorts 3 and 4 comprised 81 Australian individuals from 61 families and 219 unrelated British individuals, respectively, with probable or definite ALS diagnosed according to revised El Escorial criteria (Brooks *et al.*, 2000), with at least one relative known to have ALS and/or FTD. Individuals known to harbour mutations in causative ALS genes were excluded from analysis.

Whole-exome data from two larger patient datasets (one FTD, one ALS) were used for gene burden analysis. The FTD cohort was accessed through the International FTD Genomics Consortium (<https://ifgcsite.wordpress.com/>) and was a subset ($n = 1105$, 53.3% male) of cases examined for a genome-wide association study of FTD (Ferrari *et al.*, 2014). All cases were diagnosed with behavioural variant FTD only, i.e. no concomitant ALS. Subjects were of European ancestry and samples were collected from sites in Australia, North America and Europe via neurologist referral or (for ~3% samples) after

neuropathological diagnosis. The familial ALS cohort ($n = 1138$) was accessed through the ALS Variant Server (<http://als.umassmed.edu/>). Case and control characteristics are described in Nicolas *et al.* (2018). Cases were diagnosed with ALS and were of European ancestry, recruited at specialist clinics located in Australia, North America and Europe.

Clinical and case note review of neurological phenotypes was performed as part of baseline assessments for 16 consented patients with documented CYLD loss-of-function mutations ($n = 15$) or fitting clinical diagnostic criteria ($n = 1$) who were recruited for a clinical trial of targeted topical tumour treatment (TRAC) (Danilenko *et al.*, 2018).

Brain tissue from two sporadic corticobasal degeneration (CBD) cases was sourced from the Sydney Brain Bank for comparison with Family Aus-12 Individuals IV:5 and IV:7. Clinical and neuropathological details are provided in the Supplementary material.

This study was approved by the ethics committees of the respective institutions. Biological samples were obtained after informed consent from subjects and/or their proxies.

Genetic analysis of Family Aus-12

Microsatellite genotyping of Family Aus-12 Individual IV: 14 was performed at the Australian Genome Research Facility (Melbourne, Australia). Parametric multipoint LOD scores were calculated using MERLIN v1.1.2 (Abecasis *et al.*, 2002), with parameters detailed in the Supplementary material. Whole-genome sequencing was performed using 100-bp paired-end sequencing on the Illumina HiSeq2000 with $30\times$ coverage, by Macrogen. The Integrative Genomics Viewer was used to visualize sequencing reads [<https://software.broadinstitute.org/software/igv/>] (Thorvaldsdottir *et al.*, 2013). Analysis of intronic variants, large- and small-scale structural variants and repeat expansion was performed as described in the Supplementary material.

Immunohistochemical analysis

Formalin-fixed paraffin-embedded 10 μ m frontal cortex and hippocampal tissue sections were analysed using immunohistochemistry to determine the distribution and localization of CYLD (MABF108, mouse, Merck, 10 μ g/ml). Distribution of CYLD in these areas was visualized with DAB (3,3'-diaminobenzidine) peroxidase labelling, using Vector antigen unmasking solution prior to the Novolink Polymer Detection System (Leica, RE7140-K). Double-labelling immunofluorescence was also performed using mouse anti-CYLD and rabbit anti-TDP-43 (10782-2-AP, Protein Tech, 2 μ g/ml) and mouse anti-CYLD and rabbit anti-Human Tau (A0024, Dako, 0.4 μ g/ml). Detection was achieved using Alexa Fluor secondary antibodies followed by nuclear DAPI (4',6-diamidino-2-phenylindole) staining. Autofluorescence eliminator reagent (Merck, #2160) was used with VECTASHIELD[®] Antifade Mounting Medium (Vector Laboratories H-1000) prior to visualization on a Zeiss Axio Imager M2 Fluorescence microscope.

Mutagenesis

CYLD mutations were introduced into the pCMV6-CYLD construct (Origene) by site-directed mutagenesis using the QuikChange Lightning Site-Directed Mutagenesis Kit (Agilent).

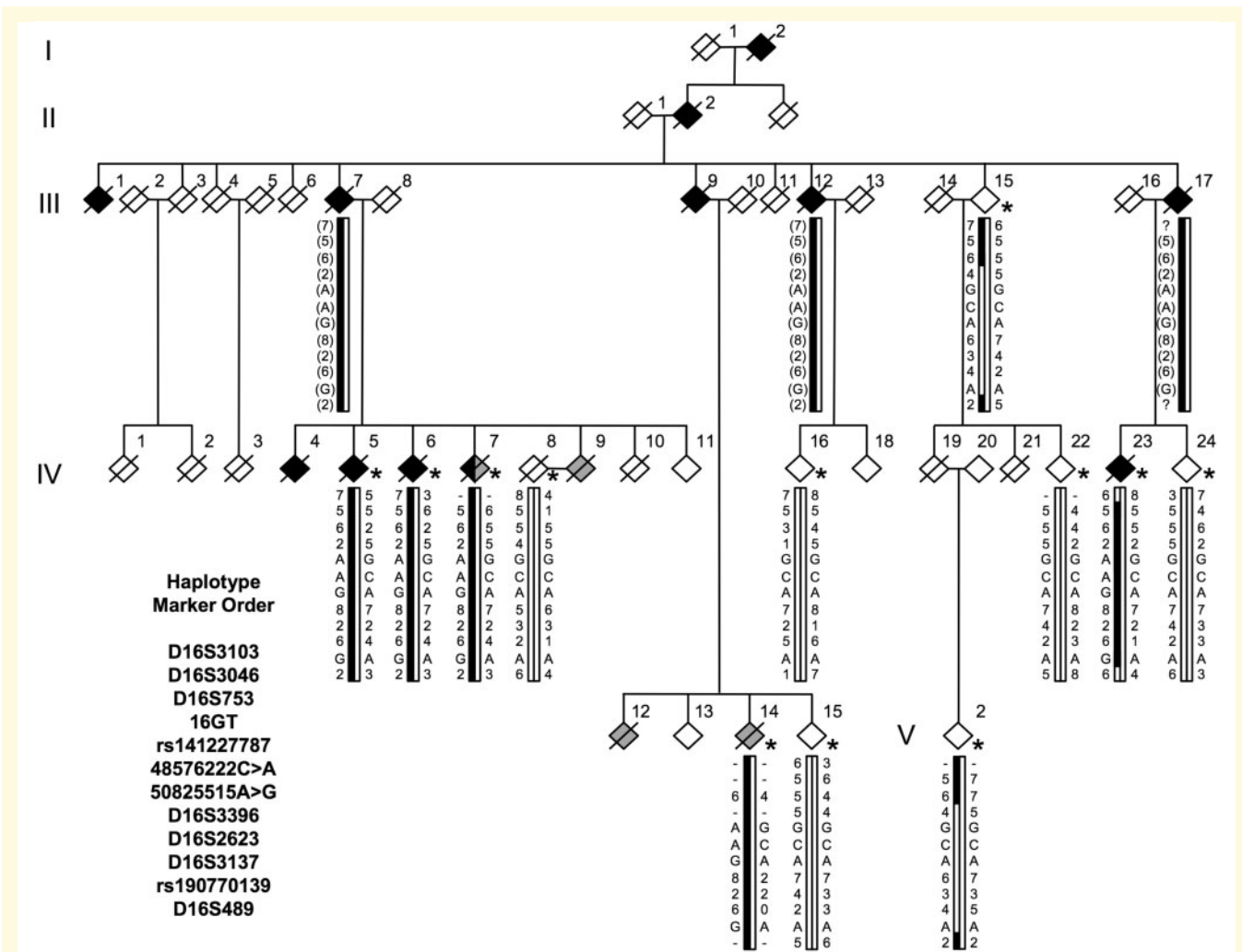


Figure 1 Family Aus-12 has a shared disease haplotype at chromosome 16p12.3–16q12.2. Black symbols show individuals with pre-senile dementia: clinically diagnosed as Alzheimer's disease (Individual II:2), FTD (Individuals IV:5, IV:7 and IV:23), or unspecified dementia (Individuals I:2, III:1, III:7, III:9, III:12, III:17, IV:4 and IV:6); grey symbols show individuals with ALS. A diagonal line indicates deceased subjects. Individuals with DNA available are indicated with an asterisk. Inferred haplotypes are in parentheses. Allele data for 12 microsatellite markers and single nucleotide variants in the region are shown, including g.50825515A>G (= *CYLD* p.M719V).

Mutated *CYLD* cDNA sequence was subcloned into pCMV6-AC, pCMV6-Entry and pCMV6-AC-GFP vectors (Origene) for expression of untagged, C-terminal myc-FLAG-tagged or C-terminal turbo green fluorescent protein (GFP)-tagged *CYLD* protein, respectively. All clones were verified by restriction digestion and sequence analysis.

Preparation of mouse primary neurons

Animal experiments were approved by the Animal Ethics Committee at Macquarie University. Primary cortical neurons were harvested from C57BL/6 mouse embryos at embryonic Days 16–18, and hippocampal neurons at embryonic Day 16.5, dissociated and plated out on to glass coverslips according to methods detailed in the [Supplementary material](#), followed by incubation at 37°C with 5% CO₂ in a humidified incubator.

TDP-43 localization analysis

After 5 days *in vitro*, mouse primary cortical neurons were transfected with constructs encoding GFP-tagged empty vector, wild-type or mutant *CYLD* using Lipofectamine 2000 (Invitrogen) following the manufacturer's instructions. Neurons were then incubated for 48 h before fixation in 4% paraformaldehyde in phosphate-buffered saline (PBS). Cells were then permeabilized with 0.1% Triton™ X-100 in PBS and non-specific background staining was blocked using 3% bovine serum albumin (BSA) in PBS. Cells were then incubated overnight at 4°C with rabbit anti-TDP-43 antibody (1:100) and mouse anti-MAP2 (1:200, ThermoFisher Scientific 13-1500) antibodies. Detection was achieved using Alexa Fluor secondary antibodies (1:300) followed by nuclear staining with 0.5 µg/ml Hoechst 33342 reagent (Sigma). Coverslips were mounted onto slides in fluorescent mounting medium (Dako) and cells were photographed with the 40× (numerical aperture = 0.75) objective on an AxioImager Z2 fluorescent microscope equipped with a

monochrome AxioCam HRm digital CCD camera (Zeiss). MAP2-positive neurons expressing GFP were counted and the proportion of GFP-expressing cells with observable cytoplasmic staining of TDP-43 was calculated. Cytoplasmic TDP-43 was scored by a researcher blind to the DNA construct used. Mean proportions were calculated from at least 50 neurons from three independent experiments.

Neuronal morphology analysis

After 3 days *in vitro*, mouse primary hippocampal neurons were transfected by incubation for 1 h with GFP-tagged constructs (1 μ l of Lipofectamine[®] 3000 reagent and 0.5 μ g of plasmid) and fixed at 72 h post-transfection with 4% paraformaldehyde. The fixed cells were permeabilized and non-specific binding blocked as described above and stained with antibodies: rabbit anti-GFP (1:1000, ab290, Abcam), mouse anti-MAP2 (1:500, M4403, Merck) and chicken anti- β -tubulin III (1:250, ab9354, Merck). Detection was achieved using Alexa Fluor[®] secondary antibodies (1:500; anti-rabbit-488, anti-mouse-647 and 1:250; anti-chicken-555). Cell nuclei were stained with DAPI (1:500, D1306, Invitrogen). Images for analysis were taken using a Zeiss Axio Imager Z1 Upright Fluorescence Microscope with a 40 \times air objective. Representative images were taken using a Zeiss 880 laser scanning microscope with a 40 \times oil objective. Images were processed using Zen 2.6 software. Axonal morphology was measured by a researcher blind to the construct used.

Deubiquitinase assay

HEK293 cells (ATCC CRL-1573) were maintained in Dulbecco's modified Eagle medium with 10% foetal bovine serum (Sigma-Aldrich) at 37°C with 5% CO₂ in a humidified incubator, and were authenticated by short tandem repeat analysis. Cells were seeded into 75 cm² flasks at 2.5 \times 10⁶ cells/flask and immediately transfected with LacZ-expressing, wild-type or mutant CYLD-mycFLAG-expressing, cDNA constructs using Lipofectamine[™] 2000 (Thermo Fisher Scientific) according to manufacturer's directions. Forty-eight hours after transfection, cells were harvested by EDTA treatment and washed in PBS. CYLD-mycFLAG protein was purified as described for the co-immunoprecipitation analyses ([Supplementary material](#)), with the addition of 1 μ g/ μ l BSA to the elution buffer. Eluted CYLD-mycFLAG was used to digest K63-linked tetra-ubiquitin or K48-linked tetra-ubiquitin chains (Enzo Life Sciences) in a reaction containing the following: 100 ng ubiquitin chains diluted in 9 μ l deubiquitinase buffer (50 mM Tris HCl pH 7.6, 5 mM dithiothreitol, 1 μ g/ μ l BSA); and 9 μ l CYLD-mycFLAG eluate. Reactions were incubated at 37°C for the specified time and stopped by addition of 5 μ l 5 \times Laemmli sample buffer and heating to 85°C for 5 min. Proteins were resolved by SDS-PAGE (sodium dodecyl sulphate-polyacrylamide gel electrophoresis) on a 12% polyacrylamide gel and immunoblotting was performed as for the co-immunoprecipitation analyses, using mouse anti-ubiquitin (MAB1510, Merck, 1:5000) or mouse anti-CYLD (1:1000) primary antibodies. Immunoblot signal intensity was quantified for each sample using ImageJ software ([Abràmoff et al., 2004](#)). The level of ubiquitin was calculated at each time point as the ratio of ubiquitin tetramer to dimer signal intensity, in order to adjust for differences in gel loading between lanes. Deubiquitinase activity was quantified by plotting log₁₀-transformed tetramer:dimer ratios from the 15-, 30- and

45-min time points and then calculating the regression slope, which represented the deubiquitinase activity of each enzyme.

NF- κ B luciferase assay

NF- κ B activity was assayed by luciferase reporter assay using the pGL4.32 construct (Promega), which expresses firefly luciferase protein under the control of a NF- κ B responsive promoter, and normalizing to *Renilla* luciferase expression from the pRL-TK construct (Promega). HEK293 cells were seeded into 96-well plates at 1.23 \times 10⁴ cells/well and transfected after 16–24 h using Lipofectamine[™] 2000 according to manufacturer's directions. Cells were co-transfected with 6.5 ng pGL4.32, 32.5 ng pRL-TK, and 40 ng untagged CYLD wild-type or mutant cDNA construct per well. Twenty-four hours after transfection, NF- κ B expression was induced by treatment with 10 pg/ μ l recombinant human tumour necrosis factor alpha (Promega) for 5 h. Induced cells were washed with PBS and luciferase expression was assayed using the Dual-Luciferase Reporter Assay System (Promega) and the CLARIOStar microplate reader (BMG Labtech), according to manufacturers' directions. For each construct combination, the ratio of NF- κ B-driven firefly luciferase activity to *Renilla* luciferase activity was calculated per well and mean firefly: *Renilla* luciferase ratio was calculated across six replicate wells.

Autophagosome maturation assay

HEK293 cells were seeded in 24-well plates containing 13-mm round coverslips. Cells were co-transfected with CYLD constructs and pBABE-puro mCherry-EGFP-LC3B (Addgene plasmid #22418) ([N'Diaye et al., 2009](#)) using Lipofectamine[™] 2000 according to manufacturer's instructions. Forty-two hours after transfection, cells were serum starved for 6 h to induce autophagy and then fixed in 4% paraformaldehyde, permeabilized with 0.1% Triton[™] X-100, and blocked with 3% BSA in PBS. Cells were then incubated with mouse anti-FLAG (1:250, Merck) at 4°C overnight. For visualization, secondary antibody Alexa Fluor[®] 647 conjugated anti-mouse (1:1000, Thermo Fisher Scientific) was used. Coverslips were mounted using fluorescence mounting medium with DAPI (Agilent). Immunofluorescence microscopy was performed using a Zeiss LSM 880 laser scanning microscope with a 100 \times /1.4 Plan-Apochrome oil objective lens. In dual-channel imaging, photo-multiplier sensitivities and offsets were set to a level at which bleed-through effects from one channel to another were negligible. All images were processed using Zen software (Carl Zeiss). Only single cells expressing both CYLD-mycFLAG and mCherry-GFP-LC3 were selected for analysis. For each cell, all autophagosomes (yellow-labelled vesicles with both mCherry and GFP tags fluorescing) and autolysosomes (red-labelled vesicles with only mCherry tag fluorescing) were counted on a merged image. Eighty-eight cells in total were scored for each construct combination across three biological replicates (at least 28 cells scored per replicate) and the mean percentage of autolysosomes was calculated as the number of red-labelled vesicles divided by the number of red- or yellow-labelled vesicles. The scorer was blind to the construct combination used.

Statistical analysis

Regression slopes of $CYLD_{wt}$ and $CYLD_{M719V}$ deubiquitinase activity were compared across 10 biological replicate assays by paired Wilcoxon signed-rank test using SPSS version 24. For NF- κ B assays, mean luciferase ratios were compared in the presence of wild-type and mutant $CYLD$ across five biological replicate assays by Student's paired-sample *t*-test using Microsoft Excel. For the TDP-43 localization assay, the mean percentage of GFP-positive neurons with cytoplasmic TDP-43 from at least 50 neurons per group across three biological replicates was compared by one-way ANOVA and Tukey's multiple comparisons test using GraphPad Prism version 7. For the neuronal morphology analyses, 20 neurons per group from two independent biological replicates were analysed and used for group comparisons. Outliers in the data were identified using the ROUT method ($Q = 1$), and data normality was tested using the Shapiro-Wilk test. Means were compared using either one-way ANOVA followed by Bonferroni's multiple comparisons test for parametric data, or a Kruskal-Wallis test followed by Dunnett's multiple comparisons test for non-parametric data, using GraphPad Prism version 8.0.2. For the autophagosome maturation assay, the mean percentage of autolysosomes was compared for $CYLD$ wild-type and mutant constructs across 88 cells by one-way ANOVA and Tukey's multiple comparisons test using GraphPad Prism version 7. Significance for all tests was set at $P < 0.05$.

Data availability

The authors are willing to provide non-identifying raw data related to this study upon request.

Results

Reclassification of Family Aus-12 Individual IV:14 and analysis of linkage

Our previous study identified a large European Australian kindred (Family Aus-12) with autosomal dominant inheritance of frontotemporal dementia and/or ALS. Presenting symptoms in family members with dementia often mimicked Alzheimer's disease but neuropathological diagnosis of two individuals confirmed that the family's dementia was due to frontotemporal lobar degeneration (FTLD) (Dobson-Stone *et al.*, 2013). Available family history at the time indicated that Individual IV:14 was unaffected. However, subsequent clinical follow-up discovered that this person had been diagnosed with ALS and had provided a blood sample for DNA studies. Microsatellite genotyping of selected chromosome 16 markers and analysis of rare single nucleotide variants from whole-exome sequencing data revealed that this person shared the 37.9 Mb common disease haplotype on chromosome 16, flanked by markers *D16S3103* and *D16S489* (Fig. 1). Multipoint linkage analysis with MERLIN including this affected individual yielded a genome-wide significant

maximum LOD score of 3.3 for markers 31447539G>A through to rs190770139 (Supplementary Table 1).

Genetic analysis of the Family Aus-12 critical region

As previously reported (Dobson-Stone *et al.*, 2013) and detailed in Supplementary Table 2, whole-exome sequencing identified only one variant that segregated with disease and was absent from public databases (dbSNP, 1000 Genomes, Exome Variant Server, gnomAD): chr16: g.50825515A>G, within the Family Aus-12 critical region, which leads to the substitution of methionine to valine at amino acid position 719 of the cylindromatosis lysine 63 deubiquitinase protein, $CYLD$ (p.M719V). As *in silico* analysis had predicted that this substitution was not likely to be pathogenic, and no $CYLD$ mutations had been reported in an independent ALS family linked to the same region (Abalkhail *et al.*, 2003), our initial conclusion was that $CYLD$ M719V was not the disease-causing variant in Family Aus-12 (Dobson-Stone *et al.*, 2013). We next performed whole-genome sequencing of DNA from affected Individuals IV:5 and IV:23, plus three unrelated controls. To ensure we had comprehensive data for all regions likely to harbour pathogenic point mutations, we performed Sanger sequencing of any low coverage exonic or proximal intronic regions within the Family Aus-12 maximal critical region. We defined 'low coverage' regions as those that were not represented by at least 10 reads in any affected individual in the whole-exome or whole-genome sequencing data. No additional exonic or canonical splice-site variants were identified that were absent in public databases, and of the six novel deep intronic variants that were identified, none were determined to affect gene splicing (Supplementary Table 3). We also screened affected individuals for structural variation using PennCNV (Wang *et al.*, 2007), Breakdancer (Chen *et al.*, 2009), STRetch (Dashnow *et al.*, 2018) and exSTra (Tankard *et al.*, 2018) algorithms. No structural variants or significant (adjusted P -value < 0.05) repeat expansions were found in common between affected individuals within the critical region. Following these analyses, $CYLD$ M719V thus remained the only novel protein-altering variant that segregated with disease.

$CYLD$ mutation analysis in clinical and neuropathological cohorts

We screened $CYLD$ coding exons and flanking intronic sequences by Sanger sequencing or examination of whole-exome or whole-genome sequencing data in two European ancestry Australian FTD or dementia cohorts ($n = 223$), a European Australian familial ALS cohort ($n = 81$ from 61 families) and a British familial ALS cohort ($n = 219$). We did not identify any additional variants predicted to affect $CYLD$ coding sequence or splicing that were absent from or with minor allele frequency (MAF) < 0.0001 in the

Genome Aggregation Database (gnomAD v2.1.1, <http://gnomad.broadinstitute.org/>) (Lek *et al.*, 2016).

We also examined CYLD variants in whole-exome data from four larger patient datasets: 1105 individuals with behavioural FTD accessed through the International FTD Genomics Consortium (<https://ifgcsite.wordpress.com/>); 1138 individuals with familial ALS at the ALS Variant Server (<http://als.umassmed.edu/>); 2800 individuals in the ALS Data Browser (<http://alsdb.org/>); and 247 familial ALS cases from the NINDS Genome-Wide Association Study of ALS (dbGaP accession no. phs000101.v5.p1). We identified 26 rare missense variants (MAF < 0.0001 in gnomAD v2.1.1 non-Finnish Europeans without neurological diseases) in ALS or FTD patients (Supplementary Table 4).

We performed gene burden testing of *CYLD* in the 1105 FTD patients relative to gnomAD non-Finnish European non-neurological exome controls ($n = 44\,779$) as implemented in the TRAPD software package (Guo *et al.*, 2018), comparing the frequency of rare (MAF < 0.0001) missense variants. To mitigate problems arising from comparison of independently processed sample cohorts, we restricted our analyses to variants of high quality (GATK Genotype Quality score ≥ 95) in positions with at least $10\times$ coverage in $\geq 90\%$ of the cohort. No enrichment of qualifying variants was observed in FTD cases (6/1105, 0.54%) relative to controls (170/44 779, 0.38%) in the whole gene (Fisher's exact test two-sided $P = 0.251$). However, analysis restricted to the deubiquitinase domain of *CYLD* (amino acids 593–948) revealed a significant enrichment (4/1105 cases, 0.36%; 47/44 779 controls, 0.10%; two-sided $P = 0.034$). A similar analysis comparing the familial ALS Variant Server cohort with 19 494 jointly called controls (Nicolas *et al.*, 2018) did not detect an enrichment of rare missense variants in *CYLD*, either in the whole gene (3/1138 cases, 0.26%; 124/19 494 controls, 0.64%; Fisher's exact test two-sided $P = 0.974$) or the deubiquitinase domain (1/1138 cases, 0.09%; 27/19 494 controls, 0.14%; $P = 0.796$).

CYLD loss-of-function mutations are not associated with dementia

CYLD cutaneous syndrome (also known as Brooke-Spiegler syndrome) is associated with heterozygous germline mutations in *CYLD* (Bignell *et al.*, 2000; Rajan and Ashworth, 2015). These patients typically develop multiple benign hair follicle tumours called cylindromas, and are not recognized to have a neurological phenotype (Rajan *et al.*, 2009). The majority of mutations in these pedigrees result in predicted truncation (Nagy *et al.*, 2015), and *CYLD* loss of heterozygosity is frequently demonstrated in cylindroma skin tumours. We reviewed the clinical files of 16 subjects with *CYLD* loss-of-function mutations, including six who were older than the maximum known age of onset for Family Aus-12 (62 years) (Supplementary Table 5). No patients met diagnostic criteria for or had been prescribed medicine to

treat dementia, and none were noted to have signs of cognitive impairment or neurological disease.

CYLD neuropathology analysis

We sought to determine whether *CYLD* showed an abnormal staining pattern in brain tissue from affected Family Aus-12 members. We have previously described the neuropathological analysis of two cases from this family: Individual IV:5, with clinical diagnosis of 'FTD with aphasia'; and Individual IV:7, with clinical diagnosis of FTD-ALS, Paget's disease and parkinsonism (Dobson-Stone *et al.*, 2013). These individuals met neuropathological criteria for both CBD FTLT with tau pathology (CBD FTLT-tau) and FTLT with type B TDP-43 pathology (type B FTLT-TDP). In the present study, we examined fixed brain tissue from Family Aus-12 Individuals IV:5 and IV:7, plus two disease control cases (one sporadic CBD FTLT-tau, and one sporadic CBD FTLT-tau with concomitant TDP-43 pathology). *CYLD* immunohistochemistry revealed staining in the blood vessels (Fig. 2A) and the cytoplasm of balloon neurons (Fig. 2B) in all cases. Both Family Aus-12 cases demonstrated widespread glial *CYLD*-immunoreactivity in the white matter, which was particularly marked in Individual IV:7 (Fig. 2D) and was absent in the sporadic cases (Fig. 2C). Patchy areas of diffuse neuronal cytoplasmic *CYLD* staining were seen in the hippocampus and the frontal cortex of Individuals IV:5 and IV:7 only (Fig. 2E). In addition, *CYLD*-immunoreactivity was seen in the nuclei of pyknotic neurons in the hippocampus and deep frontal cortex layers for the Family Aus-12 cases only, most noticeably in Individual IV:7 (Fig. 2F). Double-labelling immunofluorescence did not detect co-localization of *CYLD* with either tau or TDP-43 inclusions (Fig. 2G and H).

CYLD_{M719V} increases cytoplasmic localization of TDP-43

A cardinal neuropathological feature of half of FTD patients and almost all ALS patients, including Family Aus-12 affected members, is movement of TDP-43 from the nucleus to the cytoplasm (Neumann *et al.*, 2006; Dobson-Stone *et al.*, 2013). We examined the effect of the *CYLD*_{M719V} variant on TDP-43 localization by transfection of primary mouse cortical neurons with GFP-tagged *CYLD* wild-type (*CYLD*_{wt}) or mutant constructs and examination by immunofluorescence microscopy (Fig. 3). A significantly higher proportion of neurons transfected with *CYLD*_{wt}-GFP showed cytoplasmic TDP-43 staining ($34.4 \pm 0.5\%$ of transfected cells) relative to empty vector ($21.2 \pm 0.8\%$, one-way ANOVA with Tukey's multiple comparisons test $P = 8.8 \times 10^{-4}$) (Fig. 3B). Transfection with *CYLD*_{M719V}-GFP led to an even higher proportion of neurons with cytoplasmic TDP-43 staining ($54.9 \pm 2.7\%$, one-way ANOVA with Tukey's multiple comparisons test $P = 3.7 \times 10^{-5}$ relative to *CYLD*_{wt}-GFP). In contrast, cells transfected with

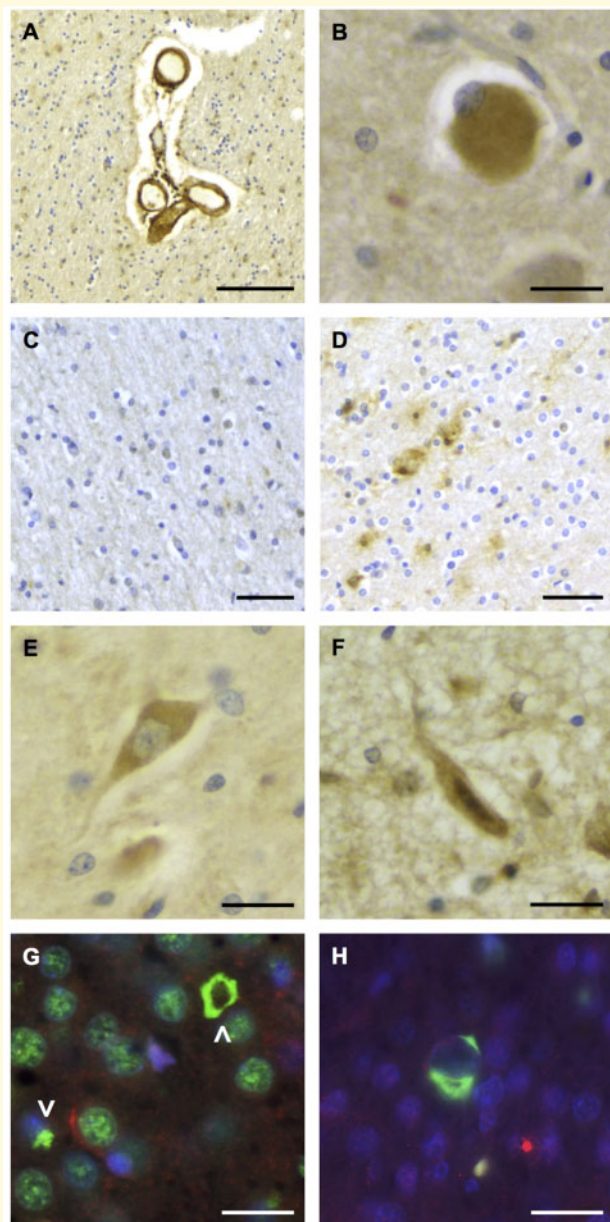


Figure 2 *CYLD*_{M719V} affects *CYLD* immunoreactivity in brain tissue. Photomicrographs demonstrating *CYLD* immunoreactivity in the frontal cortex and hippocampus. (A) Parahippocampal white matter showing *CYLD* peroxidase labelling of blood vessels, which was seen in all cases. (B) *CYLD* staining was seen in balloon neurons in all cases. Image shows representative image taken from Sydney Brain Bank Case 2. (C and D) *CYLD*-positive glia were common in Family Aus-12 (D) but not sporadic cases (C). Images were taken in the frontal white matter of Sydney Brain Bank Case 1 and Individual IV:7, respectively. (E) Diffuse, neuronal cytoplasmic *CYLD* staining of a neuron in the hippocampus of Individual IV:5. (F) *CYLD*-positive nuclear staining of a pyknotic neuron in the deep layers of the frontal cortex of Individual IV:7. (G and H) Double labelling immunofluorescence in the dentate gyrus of Individuals IV:5 (G) and IV:7 (H). TDP-43 (green, arrowheads in G) and Tau (green, H) did not co-localize with *CYLD* (red, G and H) in any case. Scale bar = 100 μm in A, 20 μm in B and E–H, 40 μm in C and D.

catalytically inactive *CYLD* cutaneous syndrome mutant *CYLD*_{D681G} (Almeida *et al.*, 2008) showed a similar proportion of cytoplasmic TDP-43-positive cells relative to the empty vector condition ($19.4 \pm 0.6\%$).

*CYLD*_{M719V} alters axonal morphology

We examined the effect of *CYLD*_{M719V} on neuronal morphology by transfection of primary mouse hippocampal neurons with GFP-tagged *CYLD* wild-type or mutant constructs and examination by immunofluorescence microscopy (Fig. 4). Overexpression of *CYLD*_{wt} led to a small non-significant decrease in primary and total axon length relative to GFP-only vector condition [mean lengths (μm) ± SEM: 781.1 ± 72.5 primary, 2120 ± 228.7 total] (Fig. 4E, H). Overexpression of *CYLD*_{M719V} led to a further decrease in primary (627.3 ± 63.5) and total axon length (1460 ± 174.4) relative to GFP-only vector, which was significant [one-way ANOVA with Bonferroni's multiple comparisons test: $P = 0.026$ (primary axon length), $P = 0.003$ (total axon length)].

*CYLD*_{M719V} does not affect interaction with TBK1, OPTN or p62

CYLD has been reported to physically interact with proteins whose genes are mutated in ALS and FTD, namely TBK1 (Friedman *et al.*, 2008), OPTN (Nagabhushana *et al.*, 2011) and p62 (Jin *et al.*, 2008). We sought to confirm these interactions and determine whether the M719V variant abrogated them by co-transfection of HEK293 cells with wild-type or mutant *CYLD*-GFP constructs and TBK1-mycFLAG, OPTN-mycFLAG, or p62-mycFLAG constructs, followed by immunoprecipitation with anti-FLAG antibody (Supplementary Fig. 1). A faint band corresponding to *CYLD*-GFP was detected in the immunoprecipitation eluate only when TBK1, OPTN or p62 was co-transfected, indicating that a small proportion of *CYLD* is bound to these proteins. An interaction was also observed with all three proteins for *CYLD* cutaneous syndrome mutant *CYLD*_{D681G} and the Family Aus-12 variant *CYLD*_{M719V}.

*CYLD*_{M719V} shows increased deubiquitinase activity

CYLD is a deubiquitinase with lysine 63 (K63) activity (Komander *et al.*, 2008). The M719V variant is located within the deubiquitinase region of *CYLD* (amino acids 593–948). We compared the deubiquitinase activity of purified *CYLD*_{wt}-mycFLAG, *CYLD*_{D681G}-mycFLAG and *CYLD*_{M719V}-mycFLAG by incubation with synthetic K63-linked ubiquitin tetramers and western blot (Fig. 5A–C and Supplementary Fig. 3A). As expected, the catalytically inactive cylindromatosis mutant *CYLD*_{D681G}-mycFLAG showed no

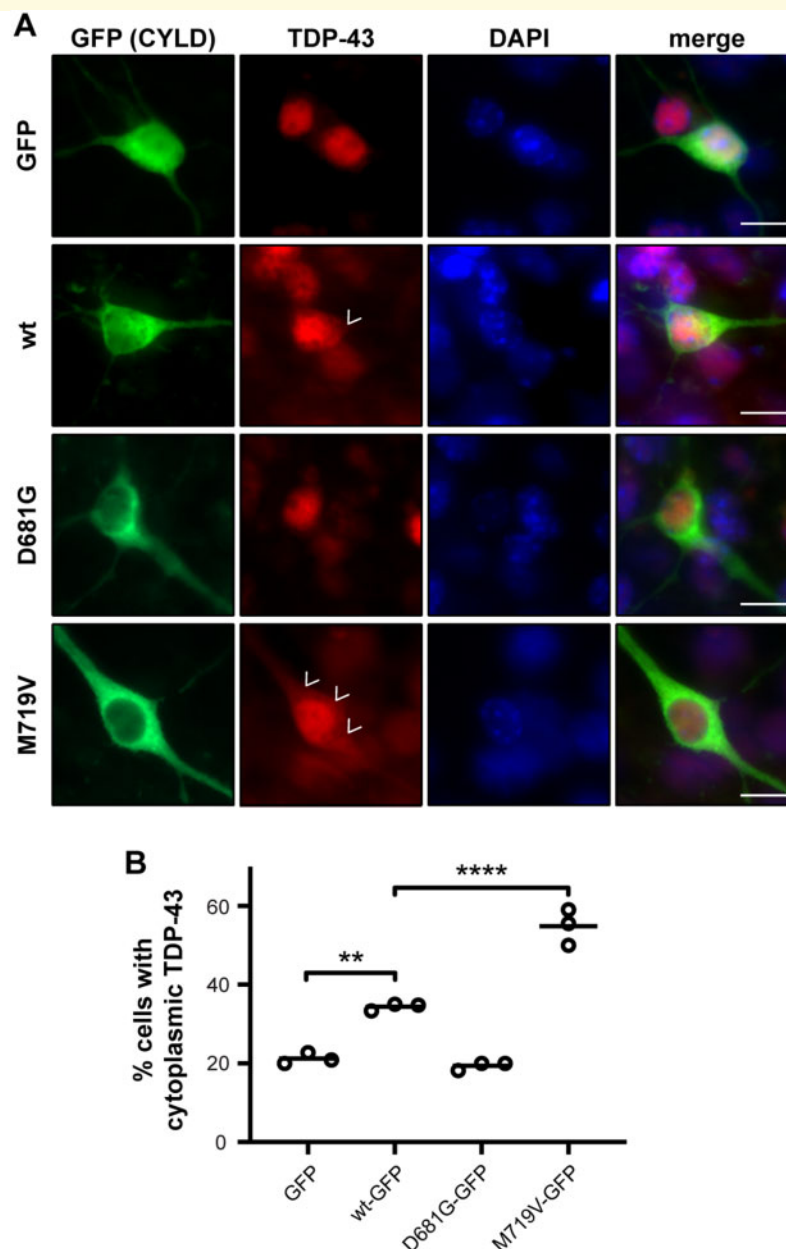


Figure 3 Expression of CYLD_{M719V} alters neuronal TDP-43 localization. (A) Representative fluorescence images of mouse cortical neurons at 7 days *in vitro*, overexpressing GFP or GFP-tagged CYLD_{wt}, CYLD_{D681G} or CYLD_{M719V} (green). TDP-43 was detected by immunofluorescent staining (red) and nuclei were visualized with DAPI (blue). Arrowheads indicate cytoplasmic TDP-43 staining in cells transfected with CYLD_{wt} and CYLD_{M719V}. (B) Quantification of the percentage of transfected cells with observable cytoplasmic TDP-43 staining, showing a significantly higher proportion of cytoplasmic TDP-43-positive cells in the CYLD_{M719V} condition relative to CYLD_{wt}. Horizontal bars indicate mean values from three independent experiments. Scale bars = 10 μ m. ** $P < 0.005$, **** $P < 0.00005$.

observable K63-deubiquitinase activity (Supplementary Fig. 3A). Interestingly, the Family Aus-12 variant CYLD_{M719V}-mycFLAG showed increased K63-deubiquitinase activity relative to CYLD_{wt}-mycFLAG (Fig. 5A), with a significant 3.7-fold increase in rate of conversion of K63-linked ubiquitin tetramers to dimers (paired Wilcoxon signed-rank test $P = 0.005$) (Fig. 5B and C). Wild-type and variant CYLD did not show observable K48-deubiquitinase activity (Supplementary Fig. 3B).

CYLD_{M719V} increases inhibition of NF- κ B

CYLD is a negative regulator of NF- κ B activity (Trompouki *et al.*, 2003). Thus we sought to determine whether the M719V variant affected CYLD's inhibition of NF- κ B by co-transfection of wild-type or mutant untagged CYLD constructs and the NF- κ B-responsive luciferase construct pGL4.32 into HEK293 cells, followed by assessment of

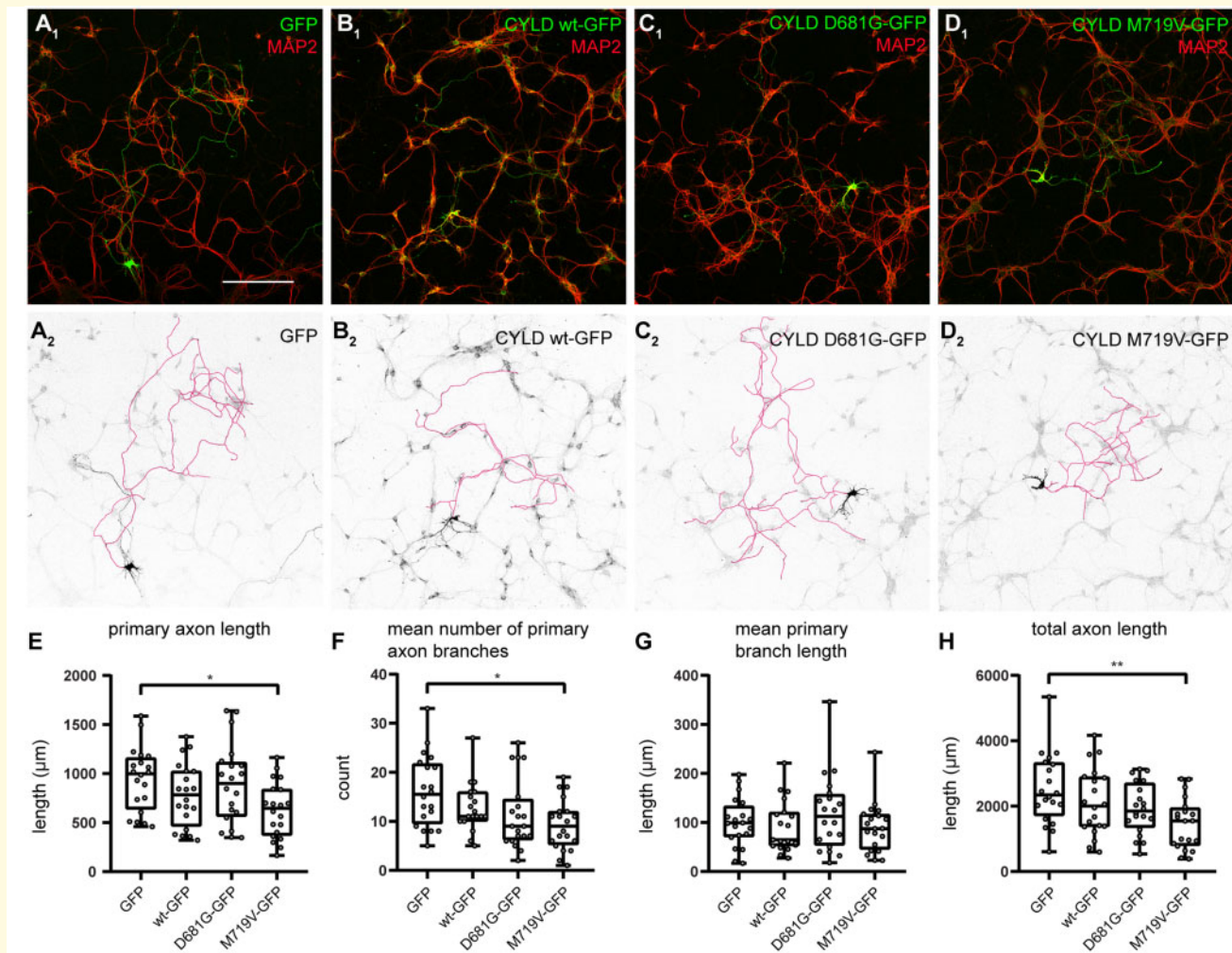


Figure 4 Expression of CYLD_{M719V} alters axonal morphology. (A₁–D₁) Representative fluorescence images of mouse hippocampal neurons at 6 days *in vitro*, overexpressing GFP (A₁), CYLD_{wt}-GFP (B₁), CYLD_{D681G}-GFP (C₁) or CYLD_{M719V}-GFP (D₁). (A₂–D₂) Inverted black and white images of GFP fluorescence of the transfected neurons shown in A₁–D₁, with pseudo-coloured axon labelling for clearer visualization of the axonal compartment. (E–H) Quantification of axonal morphology. Box plots represent median, interquartile range and minimum-maximum ($n = 20$ each group). * $P < 0.05$, ** $P < 0.005$. Scale bars = 200 μm .

luciferase activity (Fig. 5D). As expected, transfection of CYLD_{wt} led to a significant decrease in NF- κ B activity relative to empty vector control (0.26 ± 0.05 -fold, $t = 4.97$, $P = 0.008$), and transfection of cylindromatosis mutant CYLD_{D681G} led to a significant increase in NF- κ B activity relative to wild type (2.39 ± 0.27 -fold, $t = 11.43$, $P = 3.3 \times 10^{-4}$). Transfection of CYLD_{M719V} led to a significant decrease in NF- κ B activity relative to wild-type (0.50 ± 0.05 -fold, $t = 7.63$, $P = 0.002$). This increase in CYLD inhibitory activity was not due to any increase in CYLD protein levels of the M719V mutant relative to wild-type (Supplementary Fig. 5). This increased inhibitory effect on NF- κ B was recapitulated using constructs with the equivalent mutation in mouse sequence *Cyld* (0.51 ± 0.05 -fold activity of NF- κ B with *Cyld*_{M718V} relative to *Cyld*_{wt}, $t = 8.11$, $P = 0.001$) (Fig. 5D and Supplementary Fig. 5), but not in 10 other

missense variants from ALS or FTD patients (Supplementary Figs 3C and 5).

CYLD_{M719V} impairs autophagosome maturation

Several FTD-ALS proteins have been implicated in autophagy, including TBK1, OPTN and p62 (Lamark et al., 2017; Markovinic et al., 2017; Oakes et al., 2017), which interact with CYLD (Supplementary Fig. 1). We examined whether CYLD_{M719V} has an impact on this process. Autophagosome maturation was monitored at the single cell level by expressing a dual-labelled mCherry-EGFP-LC3 construct under serum starvation conditions (Fig. 6). The fusion of the autophagosome to the lysosome causes displacement

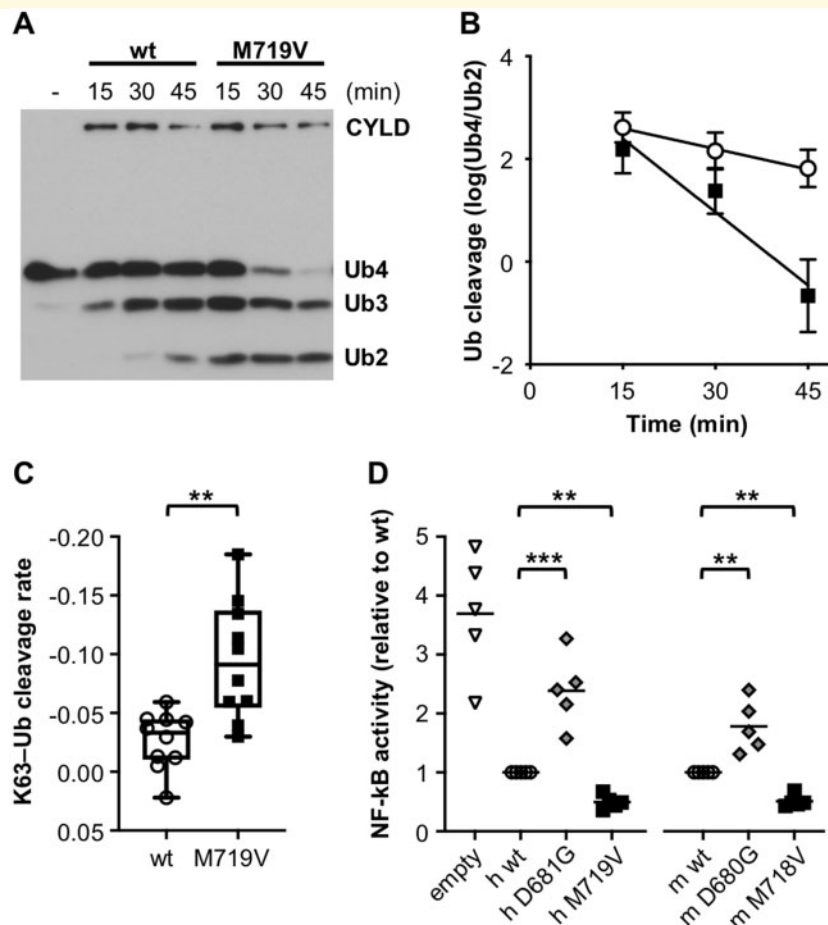


Figure 5 **CYLD_{M719V} shows increased K-63 deubiquitinase activity and inhibition of NF-κB.** K63-linked ubiquitin tetramers (Ub₄) were incubated with wild-type (wt) or M719V mutant CYLD-mycFLAG and digestion was observed. **(A)** Representative immunoblot showing appearance of bands corresponding to ubiquitin trimers (Ub₃) and dimers (Ub₂) after 15, 30 and 45 min of CYLD treatment. An uncropped image of this blot is available in [Supplementary Fig. 4](#). **(B)** Quantification of ubiquitin cleavage expressed as log₁₀-transformed Ub₄/Ub₂ after treatment with CYLD_{wt} (open circles) or CYLD_{M719V} (filled squares) (mean ± SEM from 10 experiments). **(C)** Comparison of rate of K63-ubiquitin cleavage shows significantly increased rate of cleavage for CYLD_{M719V} relative to CYLD_{wt}. Box plots represent median, interquartile range and minimum-maximum from *n* = 10 independent experiments. **(D)** Quantification of NF-κB activity. HEK293 cells were transfected with NF-κB-responsive luciferase construct pGL4.32 plus empty vector or human (h) CYLD_{wt}, CYLD_{D681G} or CYLD_{M719V} constructs or mouse (m) equivalents Cyld_{wt}, Cyld_{D680G} or Cyld_{M718V}, and NF-κB expression was induced by tumour necrosis factor α treatment. Horizontal bars indicate mean values from five independent experiments. Values are normalized to human CYLD_{wt} or mouse Cyld_{wt}, and show significant increases for cylindromatosis mutant CYLD_{D681G} and mouse equivalent Cyld_{D680G} and decreases for Family Aus-12 mutant CYLD_{M719V} and mouse equivalent Cyld_{M718V}. ***p* < 0.005, ****p* < 0.0005.

of its contents within the acidic environment of the lysosome for degradation, resulting in quenching of the EGFP but not the mCherry signal for the mCherry-EGFP-LC3 reporter. Thus, co-localization of both mCherry and GFP fluorescence is indicative of improper fusion of the autophagosome to the lysosome, whereas mCherry fluorescence alone corresponds to proper fusion and mature autolysosome (Klionsky *et al.*, 2016). A significantly increased proportion of autophagosomes and concomitant decreased proportion of autolysosomes were observed in cells co-transfected with mCherry-EGFP-LC3 and CYLD_{M719V}-mycFLAG compared to cells that were co-transfected with CYLD_{wt}-mycFLAG (one-way ANOVA with Tukey's multiple comparisons test

P < 10⁻⁴) (Fig. 6B). This suggests that autophagosome fusion is impaired in CYLD_{M719V}-mycFLAG-transfected cells.

Discussion

We demonstrate here that the M719V missense variant in CYLD segregates with disease in a large multigenerational FTD-ALS family. This variant is associated with altered CYLD immunoreactivity in brain tissue and significantly impacts two key roles of CYLD: K63 deubiquitination (Komander *et al.*, 2008) and negative regulation of NF-κB (Trompouki *et al.*, 2003). Furthermore, *in vitro* expression

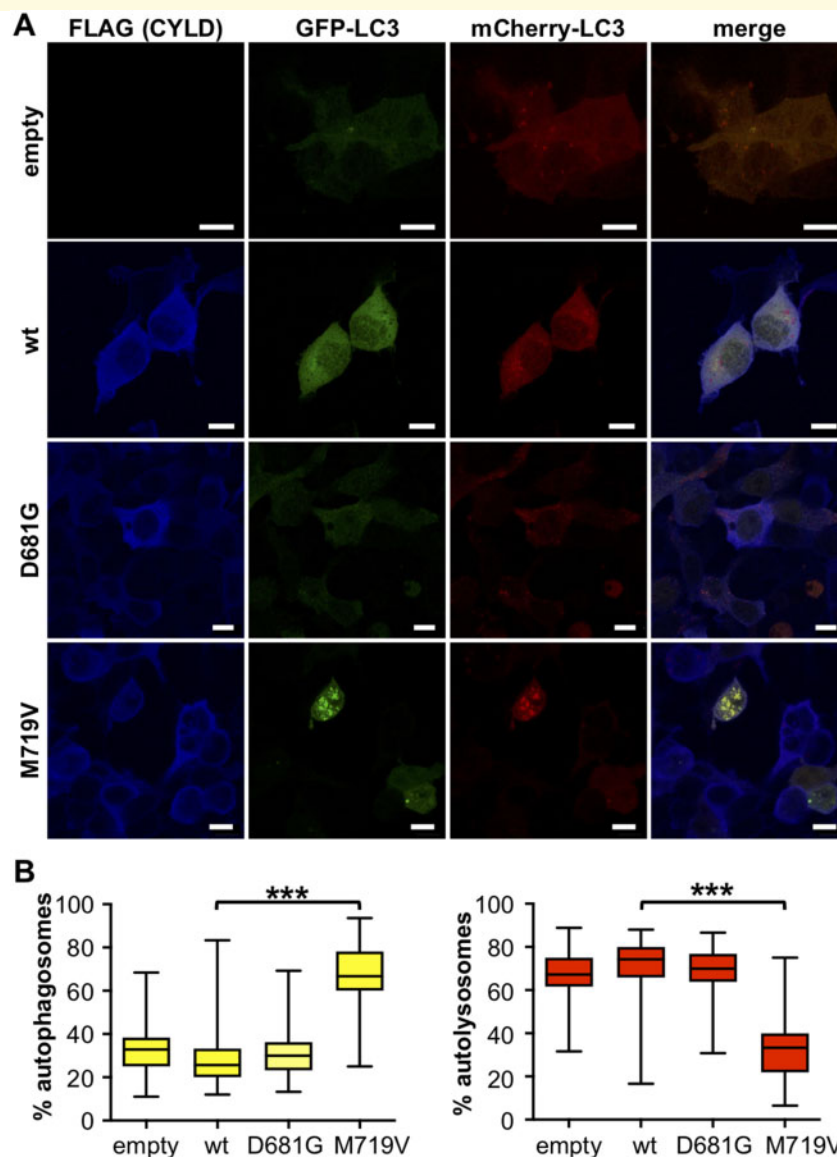


Figure 6 $CYLD_{M719V}$ impairs fusion of autophagosomes with lysosomes. **(A)** Images of HEK293 cells cotransfected with tandem mCherry-GFP-tagged autophagy marker LC3 plus empty vector or mycFLAG-tagged $CYLD_{wt}$, $CYLD_{D681G}$ or $CYLD_{M719V}$ constructs. Cells were serum starved for 6 h to induce autophagy. Fusion of the autophagosome with the lysosome to produce autolysosomes quenches GFP but not mCherry fluorescence. In the merged image, autophagosomes appear as yellow vesicles, while autolysosomes appear as red vesicles. **(B)** Quantification of the percentage of autophagosomes (mCherry- and GFP-positive vesicles, left) and autolysosomes (mCherry-positive only vesicles, right) relative to total vesicle number, showing a significant decrease in proportion of autolysosomes in $CYLD_{M719V}$ cells, but not $CYLD_{D681G}$ cells relative to $CYLD_{wt}$. Box plots represent median, interquartile range and minimum-maximum ($n = 88$ each group). Scale bar = 10 μm . *** $P < 0.0001$.

of $CYLD_{M719V}$ recapitulates two cellular phenotypes of FTD and ALS: increased cytoplasmic TDP-43 (Neumann et al., 2006) and impaired autophagy (Deng et al., 2017; Evans and Holzbaur, 2019). As we did not have DNA available from relatives of other $CYLD$ variant carriers, we were only able to demonstrate disease segregation of a $CYLD$ mutation in one family, which is a limitation of this study, albeit not unusual for modern FTD and ALS gene identification studies (Williams et al., 2016). However, our observations of genome-wide significant linkage in this

family, exclusion of other genomic variants in the linked region, and our neuropathological and *in vitro* analyses of $CYLD_{M719V}$, together indicate that mutation of $CYLD$ is a cause of FTD-ALS.

No mutations were identified in the coding or flanking intronic regions of $CYLD$ in a previously reported ALS family linked to an overlapping region on chromosome 16 (Abalkhail et al., 2003; Dobson-Stone et al., 2013). We note that the maximal LOD score for this family of 2.06 was suggestive but not statistically genome-wide significant, and a

third family initially reported to be linked to this locus with maximal LOD score of 2.1 (Family F2 in Ruddy *et al.*, 2003) was subsequently shown to exhibit genome-wide significant linkage to chromosome 9p, with affected family members all harbouring the pathogenic *C9orf72* repeat expansion (Al-Sarraj *et al.*, 2011).

We observed differences in CYLD immunostaining in CYLD mutation carriers relative to sporadic CBD cases, most notably widespread staining of glia in the white matter. CYLD was not observed in cytoplasmic inclusions, which contrasts with findings for mutation carriers of some other FTD-ALS genes [e.g. *OPTN* (Maruyama *et al.*, 2010), *SQSTM1* (Teyssou *et al.*, 2013)] but not all [e.g. *TBK1* (Pottier *et al.*, 2015), *TIA1* (Hirsch-Reinschagen *et al.*, 2017)]. We previously reported that Family Aus-12 Individuals IV:5 and IV:7 met neuropathological criteria for both FTLT-TDP type B and CBD FTLT-tau (Dobson-Stone *et al.*, 2013). TDP-43 deposition is characteristic of most other reported FTD-ALS genes (Maruyama *et al.*, 2010; DeJesus-Hernandez *et al.*, 2011; Teyssou *et al.*, 2013; Pottier *et al.*, 2015). However, it is of note that concomitant TDP-43 and tau pathology has also been reported in 3/11 *TBK1* mutation carriers with neuropathological data reported thus far: one exhibited tau-immunoreactive tufted astrocytes and neuronal cytoplasmic inclusions (Van Mossevelde *et al.*, 2016), and two exhibited argyrophilic grain disease (Koriath *et al.*, 2017; van der Zee *et al.*, 2017). Three cases showed no tau pathology (Van Mossevelde *et al.*, 2016; van der Zee *et al.*, 2017), and tau neuropathological analysis was not reported for the remaining five cases (Freischmidt *et al.*, 2015; Pottier *et al.*, 2015). Neuropathological examination of more CYLD and *TBK1* mutation carriers will be required before concluding whether this is a chance finding, or indicative of some common predisposition for these mutations to cause abnormal deposition of tau in addition to TDP-43.

The CYLD_{M719V} mutation leads to a significant increase in K63 deubiquitinase activity and inhibition of NF-κB. This is in contrast to CYLD missense mutations reported in cylindromatosis and similar disorders, which severely reduce or abrogate deubiquitinase activity and NF-κB inhibition (Blake and Toro, 2009), implying a different pathogenetic mechanism for these disorders. Consistent with this hypothesis, we found no evidence of neurological disease in patients with CYLD loss-of-function mutations, including six who were older than the maximum known age of onset for Family Aus-12. Conversely, review of available clinical records did not reveal any signs of a skin disorder in affected individuals from Family Aus-12, although we cannot exclude more subtle manifestations of CYLD cutaneous syndrome, such as milia (Bajwa *et al.*, 2018). Our data are thus consistent with opposing effects of gain-of-function versus loss-of-function mutations for the same gene, as has been observed previously for other genes (e.g. *SMCHD1*; Gurzau *et al.*, 2018).

We observed that overexpression of CYLD_{M719V} led to mislocalization of TDP-43 to the cytoplasm in primary neurons. No TDP-43-positive inclusions were observed, in

contrast with similar studies performed with some other FTD and ALS genes, e.g. *CHCHD10* (Woo *et al.*, 2017) and *PFN1* (Tanaka *et al.*, 2016); but not all, e.g. *VCP* (Ritson *et al.*, 2010). Diffuse cytoplasmic staining of TDP-43 is seen as a precursor to aggregate formation (Brandmeir *et al.*, 2008; Mori *et al.*, 2008; Kim *et al.*, 2019): it is possible that longer-term transfection of mutant CYLD would lead to observable aggregation of TDP-43. We also observed that neuronal overexpression of CYLD_{M719V} led to a reduction of axonal length, which has been observed before with mutant ALS proteins, e.g. *SOD1* (Takeuchi *et al.*, 2002), *PFN1* (Wu *et al.*, 2012) and TDP-43 (Duan *et al.*, 2011; Tripathi *et al.*, 2014). The latter observation indicates that axonal morphology effects of CYLD_{M719V} might be mediated through altering TDP-43 localization. However, further studies would be needed to demonstrate whether there is a causal relationship between TDP-43 localization and altered axonal morphology as a result of CYLD_{M719V} expression. Both increased K63 deubiquitinase activity and inhibition of NF-κB may contribute to the reduced axonal growth in CYLD_{M719V}-expressing neurons. For example, K63 ubiquitination of muscleblind-like protein 1 (MBNL1) has recently been shown to be important for its localization to the cytoplasm, and promotion of axonal growth (Wang *et al.*, 2018). K63 deubiquitination negatively regulates MBNL1 function and could contribute to the reduced axonal growth. Furthermore, NF-κB is a key regulator in mediating signalling cues that promote axonal growth (reviewed in Gutierrez and Davies, 2011) and increased inhibition of NF-κB may be a major factor, leading to the observed axonal phenotype in our study.

We confirmed that CYLD directly interacts with *TBK1*, *OPTN* and p62 (Friedman *et al.*, 2008; Jin *et al.*, 2008; Zhang *et al.*, 2008; Nagabhushana *et al.*, 2011), three proteins that are encoded by genes with mutations in FTD or ALS. Nagabhushana *et al.* (2011) reported that interaction between *OPTN* and CYLD is required for CYLD-mediated inhibition of NF-κB. The interaction of p62 with CYLD is required for the negative regulation of osteoclastogenesis (Jin *et al.*, 2008). Lastly, CYLD and *TBK1* are substrates of each other. CYLD negatively regulates *TBK1*-mediated antiviral innate immunity by removal of K63 ubiquitin chains from *TBK1* (Friedman *et al.*, 2008; Zhang *et al.*, 2008). Conversely, CYLD phosphorylation by *TBK1* has been observed upon T-cell receptor stimulation (Lork *et al.*, 2018).

It is pertinent that *TBK1*, *OPTN* and p62 are all implicated in autophagy (Wild *et al.*, 2011; Pilli *et al.*, 2012; Lamark *et al.*, 2017; Markovinic *et al.*, 2017) and that ALS and/or FTD-causative mutations in these and other genes impair autophagic function (Soo *et al.*, 2015; Moore and Holzbaur, 2016; Webster *et al.*, 2016; Lee *et al.*, 2018). In the current study, expression of CYLD_{M719V} led to a significant decrease in relative autolysosome numbers compared to CYLD_{wt} and concomitant increase in autophagosomes. This suggests that CYLD_{M719V} leads to an impairment in autophagosome maturation to autolysosomes. We hypothesize that overactive

CYLD is another mechanism by which autophagy can become impaired in FTD and ALS.

CYLD has not hitherto been extensively studied in a neuronal context, but is highly enriched in the postsynaptic density (Dosemeci *et al.*, 2013; Jin *et al.*, 2019) and mediates long-term depression in cultured neurons, likely through deubiquitination of the synaptic scaffold protein PSD-95 (Ma *et al.*, 2017). Recently, CYLD was identified as a mediator of programmed necroptosis in neurons *in vitro*, and post-traumatic brain injury neuronal death *in vivo* (Ganjam *et al.*, 2018). It is therefore possible that the overactive CYLD_{M719V} mutant may at least in part lead to neurodegeneration via inappropriate necroptosis of neurons.

CYLD is a highly constrained gene (more intolerant to missense substitutions than 93% of genes; Lek *et al.*, 2016) and mutations that increase its activity are likely extremely rare. We observed a statistically significant enrichment of CYLD deubiquitinase domain missense variants in individuals with FTD but not ALS. We note that gene burden tests in large case-control exome studies reliably detect enrichment of rare variants in major familial ALS genes such as *SOD1* and *TARDBP* (Cirulli *et al.*, 2015). However, rarer ALS genes, even those with previously demonstrated strong linkage and/or segregation in large pedigrees, often fail burden testing, e.g. *PFN1*, *VAPB*, *MATR3* (Cirulli *et al.*, 2015). Conversely, none of the CYLD variants we assayed apart from M719V showed a significant increase of NF-κB inhibition. This implies that either the enrichment in FTD patients is a chance observation, or that some FTD- or ALS-associated CYLD variants are pathogenic but do not act by affecting NF-κB inhibition. As we only examined cohorts with European ancestry, we cannot comment on the possible contribution of CYLD mutations to non-European FTD or ALS cohorts.

In conclusion, we have demonstrated that mutation of CYLD is a cause of FTD and ALS. Although CYLD mutations appear to be rare, its interaction with at least three other proteins encoded by established FTD and ALS genes suggests that CYLD also plays a central role in autophagy pathways contributing to the pathogenesis of these disorders. Further work on the central role of autophagy in FTD and ALS should be the focus of future studies.

Acknowledgements

We would like to thank Paul Leo and Matthew Brown for access to control exome data. We thank the International FTD-Genomics Consortium (IFGC; <https://ifgcsite.wordpress.com/>) for providing allele-count information. IFGC is supported by intramural funding from the National Institute of Neurological Disorders and Stroke (NINDS) and National Institute on Aging (NIA), and Alzheimer's Society (grant 284). The authors would like to thank the ALS Variant Server, which is supported by funds from NIH/NINDS (1R01NS065847), AriSLA (EXOMEFALS, NOVALS), the ALS Association, and the Motor Neuron Disease (MND)

Association. This research was undertaken with the assistance of resources from the National Computational Infrastructure, which is supported by the Australian Government. Data used in this research were in part obtained from the UK MND Collections for MND Research, funded by the MND Association and the Wellcome Trust. We would like to thank Family Aus-12 family members, and other people with FTD or ALS and their families, for their participation in this project. Tissues were received from: the Sydney Brain Bank at Neuroscience Research Australia, which is supported by The University of New South Wales and Neuroscience Research Australia; and the South Australian Brain Bank, which is supported by Flinders University and the Flinders Foundation. Disclaimer: this publication presents independent research in part commissioned by the Health Innovation Challenge Fund (HICF-R7-395), a parallel funding partnership between the Wellcome Trust and the Department of Health. The views expressed in this publication are those of the author(s) and not necessarily those of the Wellcome Trust or the Department of Health.

Funding

This research was funded by the National Health and Medical Research Council of Australia (NHMRC) Project Grants 1062539 (to C.D.S. and J.B.K.), 1140708 (to C.D.S., J.B.K., I.P.B. and J.D.A.) and 1083209 (to T.F.), and Dementia Research Team Grant 1095215 (to I.P.B., J.D.A., J.B.K., C.D.S.) and by funding to ForeFront, a collaborative research group dedicated to the study of FTD and MND, from the NHMRC (1037746, 1095127, 1132524). C.D.S. is funded by an NHMRC Boosting Dementia Research Leadership Fellowship (1138223) and the University of Sydney. T.F. is supported by an Australian Research Council Discovery Project Grant (180101473). J.M.F. and A.D.S. were supported by NHMRC Project Grant 1063960 (to J.M.F. and P.R.S.), and J.M.F. was additionally supported by the Janette Mary O'Neil Research Fellowship. N.R. is funded by a Wellcome Trust Intermediate Clinical Fellowship (WT097163MA), the Wellcome Trust and UK Department of Health under the Health Innovation Challenge Fund (100935/Z/13/Z), the Newcastle NIHR Biomedical Research Centre (BRC) and the Newcastle MRC/EPSRC Molecular Pathology Node. M.F.B. and M.B. were supported by the Victorian Government's Operational Infrastructure Support Program and the NHMRC Independent Research Institute Infrastructure Support Scheme. M.B. was also supported by NHMRC Program Grant (1054618) and NHMRC Senior Research Fellowship (1102971). Funding was provided to J.E.L. by US National Institutes of Health (NIH)/National Institute of Neurological Disorders and Stroke (NINDS) (R01NS073873) and the American ALS Association. O.P. is supported by an NHMRC Senior Research Fellowship (1103258). G.M.H. holds an NHMRC Senior Principal Research Fellowship

(1079679). K.L.W. was supported by a University of Sydney Postgraduate Scholarship during this research.

Competing interests

The authors report no competing interests.

Supplementary material

Supplementary material is available at *Brain* online.

References

- Abalkhail H, Mitchell J, Habgood J, Orrell R, de Bellerocche J. A new familial amyotrophic lateral sclerosis locus on chromosome 16q12.1-16q12.2. *Am J Hum Genet* 2003; 73: 383–9.
- Abecasis GR, Cherny SS, Cookson WO, Cardon LR. Merlin–rapid analysis of dense genetic maps using sparse gene flow trees. *Nat Genet* 2002; 30: 97–101.
- Abrmoff MD, Magalhães PJ, Ram SJ. Image processing with ImageJ. *Biophotonics Int* 2004; 11: 36–42.
- Al-Sarraj S, King A, Troakes C, Smith B, Maekawa S, Bodi I, et al. p62 positive, TDP-43 negative, neuronal cytoplasmic and intranuclear inclusions in the cerebellum and hippocampus define the pathology of C9orf72-linked FTL and MND/ALS. *Acta Neuropathol* 2011; 122: 691–702.
- Almeida S, Maillard C, Itin P, Hohl D, Huber M. Five new CYLD mutations in skin appendage tumors and evidence that aspartic acid 681 in CYLD is essential for deubiquitinase activity. *J Invest Dermatol* 2008; 128: 587–93.
- Bajwa DS, Nasr B, Carmichael AJ, Rajan N. Milia: a useful clinical marker of CYLD mutation carrier status. *Clin Exp Dermatol* 2018; 43: 193–5.
- Baker M, Mackenzie IR, Pickering-Brown SM, Gass J, Rademakers R, Lindholm C, et al. Mutations in progranulin cause tau-negative frontotemporal dementia linked to chromosome 17. *Nature* 2006; 442: 916–9.
- Bignell GR, Warren W, Seal S, Takahashi M, Rapley E, Barfoot R, et al. Identification of the familial cylindromatosis tumour-suppressor gene. *Nat Genet* 2000; 25: 160–5.
- Blake PW, Toro JR. Update of cylindromatosis gene (CYLD) mutations in Brooke-Spiegler syndrome: novel insights into the role of deubiquitination in cell signaling. *Hum Mutat* 2009; 30: 1025–36.
- Brandmeir NJ, Geser F, Kwong LK, Zimmerman E, Qian J, Lee VM, et al. Severe subcortical TDP-43 pathology in sporadic frontotemporal lobar degeneration with motor neuron disease. *Acta Neuropathol* 2008; 115: 123–31.
- Brooks BR, Miller RG, Swash M, Munsat TL; World Federation of Neurology Research Group on Motor Neuron Diseases. El Escorial revisited: revised criteria for the diagnosis of amyotrophic lateral sclerosis. *Amyotroph Lateral Scler Other Motor Neuron Disord* 2000; 1: 293–9.
- Chen K, Wallis JW, McLellan MD, Larson DE, Kalicki JM, Pohl CS, et al. BreakDancer: an algorithm for high-resolution mapping of genomic structural variation. *Nat Methods* 2009; 6: 677–81.
- Cirulli ET, Lasseigne BN, Petrovski S, Sapp PC, Dion PA, Leblond CS, et al. Exome sequencing in amyotrophic lateral sclerosis identifies risk genes and pathways. *Science* 2015; 347: 1436–41.
- Danilenko M, Stamp E, Stocken DD, Husain A, Zangarini M, Cranston A, et al. Targeting tropomyosin receptor kinase in cutaneous CYLD defective tumors with pegcantratinib: the TRAC randomized clinical trial. *JAMA Dermatol* 2018; 154: 913–21.
- Dashnow H, Lek M, Phipson B, Halman A, Sadedin S, Lonsdale A, et al. STRetch: detecting and discovering pathogenic short tandem repeat expansions. *Genome Biol* 2018; 19: 121.
- DeJesus-Hernandez M, Mackenzie IR, Boeve BF, Boxer AL, Baker M, Rutherford NJ, et al. Expanded GGGGCC hexanucleotide repeat in noncoding region of C9ORF72 causes chromosome 9p-linked FTD and ALS. *Neuron* 2011; 72: 245–56.
- Deng Z, Sheehan P, Chen S, Yue Z. Is amyotrophic lateral sclerosis/frontotemporal dementia an autophagy disease? *Mol Neurodegener* 2017; 12: 90.
- Dobson-Stone C, Luty AA, Thompson EM, Blumbergs P, Brooks WS, Short CL, et al. Frontotemporal dementia-amyotrophic lateral sclerosis syndrome locus on chromosome 16p12.1-q12.2: genetic, clinical and neuropathological analysis. *Acta Neuropathol* 2013; 125: 523–33.
- Dosemeci A, Thein S, Yang Y, Reese TS, Tao-Cheng JH. CYLD, a deubiquitinase specific for lysine63-linked polyubiquitins, accumulates at the postsynaptic density in an activity-dependent manner. *Biochem Biophys Res Commun* 2013; 430: 245–9.
- Duan W, Guo Y, Jiang H, Yu X, Li C. MG132 enhances neurite outgrowth in neurons overexpressing mutant TAR DNA-binding protein-43 via increase of HO-1. *Brain Res* 2011; 1397: 1–9.
- Evans CS, Holzbaur ELF. Autophagy and mitophagy in ALS. *Neurobiol Dis* 2019; 122: 35–40.
- Fecto F, Yan J, Vemula SP, Liu E, Yang Y, Chen W, et al. SQSTM1 mutations in familial and sporadic amyotrophic lateral sclerosis. *Arch Neurol* 2011; 68: 1440–6.
- Ferrari R, Hernandez DG, Nalls MA, Rohrer JD, Ramasamy A, Kwok JB, et al. Frontotemporal dementia and its subtypes: a genome-wide association study. *Lancet Neurol* 2014; 13: 686–99.
- Freischmidt A, Wieland T, Richter B, Ruf W, Schaeffer V, Müller K, et al. Haploinsufficiency of TBK1 causes familial ALS and frontotemporal dementia. *Nat Neurosci* 2015; 18: 631–6.
- Friedman CS, O'Donnell MA, Legarda-Addison D, Ng A, Cardenas WB, Yount JS, et al. The tumour suppressor CYLD is a negative regulator of RIG-I-mediated antiviral response. *EMBO Rep* 2008; 9: 930–6.
- Ganjam GK, Terpolilli NA, Diemert S, Eisenbach I, Hoffmann L, Reuther C, et al. Cylindromatosis mediates neuronal cell death in vitro and in vivo. *Cell Death Differ* 2018; 25: 1394–407.
- Goldman JS, Farmer JM, Wood EM, Johnson JK, Boxer A, Neuhaus J, et al. Comparison of family histories in FTL subtypes and related tauopathies. *Neurology* 2005; 65: 1817–9.
- Guo MH, Plummer L, Chan YM, Hirschhorn JN, Lippincott MF. Burden testing of rare variants identified through exome sequencing via publicly available control data. *Am J Hum Genet* 2018; 103: 522–34.
- Gurzau AD, Chen K, Xue S, Dai W, Lucet IS, Ly TTN, et al. FSHD2- and BAMS-associated mutations confer opposing effects on SMCHD1 function. *J Biol Chem* 2018; 293: 9841–53.
- Gutierrez H, Davies AM. Regulation of neural process growth, elaboration and structural plasticity by NF-kappaB. *Trends Neurosci* 2011; 34: 316–25.
- Hirsch-Reinshagen V, Pottier C, Nicholson AM, Baker M, Hsiung GR, Krieger C, et al. Clinical and neuropathological features of ALS/FTD with TIA1 mutations. *Acta Neuropathol Commun* 2017; 5: 96.
- Hutton M, Lendon CL, Rizzu P, Baker M, Froelich S, Houlden H, et al. Association of missense and 5'-splice-site mutations in tau with the inherited dementia FTDP-17. *Nature* 1998; 393: 702–5.
- Jin C, Kim S, Kang H, Yun KN, Lee Y, Zhang Y, et al. Shank3 regulates striatal synaptic abundance of Cyld, a deubiquitinase specific for Lys63-linked polyubiquitin chains. *J Neurochem* 2019; 150: 776–86.
- Jin W, Chang M, Paul EM, Babu G, Lee AJ, Reiley W, et al. Deubiquitinating enzyme CYLD negatively regulates RANK signaling and osteoclastogenesis in mice. *J Clin Invest* 2008; 118: 1858–66.

- Kim G, Bolbolan K, Shahidehpour R, Jamshidi P, Gefen T, Ayala IA, et al. Morphology and distribution of TDP-43 pre-inclusions in primary progressive aphasia. *J Neuropathol Exp Neurol* 2019; 78: 229–37.
- Klionsky DJ, Abdelmohsen K, Abe A, Abedin MJ, Abeliovich H, Acevedo Arozena A, et al. Guidelines for the use and interpretation of assays for monitoring autophagy (3rd edition). *Autophagy* 2016; 12: 1–222.
- Komander D, Lord CJ, Scheel H, Swift S, Hofmann K, Ashworth A, et al. The structure of the CYLD USP domain explains its specificity for Lys63-linked polyubiquitin and reveals a B box module. *Mol Cell* 2008; 29: 451–64.
- Koriath CA, Bocchetta M, Brotherhood E, Woollacott IO, Norsworthy P, Simon-Sanchez J, et al. The clinical, neuroanatomical, and neuropathologic phenotype of TBK1-associated frontotemporal dementia: a longitudinal case report. *Alzheimers Dement (Amst)* 2017; 6: 75–81.
- Lamark T, Svenning S, Johansen T. Regulation of selective autophagy: the p62/SQSTM1 paradigm. *Essays Biochem* 2017; 61: 609–24.
- Lee A, Rayner SL, Gwee SSL, De Luca A, Shahheydari H, Sundaramoorthy V, et al. Pathogenic mutation in the ALS/FTD gene, CCNF, causes elevated Lys48-linked ubiquitylation and defective autophagy. *Cell Mol Life Sci* 2018; 75: 335–54.
- Lek M, Karczewski KJ, Minikel EV, Samocha KE, Banks E, Fennell T, et al. Analysis of protein-coding genetic variation in 60,706 humans. *Nature* 2016; 536: 285–91.
- Lillo P, Hodges JR. Frontotemporal dementia and motor neurone disease: overlapping clinic-pathological disorders. *J Clin Neurosci* 2009; 16: 1131–5.
- Lork M, Kreike M, Staal J, Beyaert R. Importance of validating antibodies and small compound inhibitors using genetic knockout studies—T cell receptor-induced CYLD phosphorylation by IKKepsilon/TBK1 as a case study. *Front Cell Dev Biol* 2018; 6: 40.
- Ma Q, Ruan H, Peng L, Zhang M, Gack MU, Yao WD. Proteasome-independent polyubiquitin linkage regulates synapse scaffolding, efficacy, and plasticity. *Proc Natl Acad Sci USA* 2017; 114: E8760–9.
- Mackenzie IR, Nicholson AM, Sarkar M, Messing J, Purice MD, Pottier C, et al. TIA1 mutations in amyotrophic lateral sclerosis and frontotemporal dementia promote phase separation and alter stress granule dynamics. *Neuron* 2017; 95: 808–16.e9.
- Markovinic A, Cimbri R, Ljutic T, Kriz J, Rogelj B, Munitic I. Optineurin in amyotrophic lateral sclerosis: multifunctional adaptor protein at the crossroads of different neuroprotective mechanisms. *Prog Neurobiol* 2017; 154: 1–20.
- Maruyama H, Morino H, Ito H, Izumi Y, Kato H, Watanabe Y, et al. Mutations of optineurin in amyotrophic lateral sclerosis. *Nature* 2010; 465: 223–6.
- Moore AS, Holzbaur EL. Dynamic recruitment and activation of ALS-associated TBK1 with its target optineurin are required for efficient mitophagy. *Proc Natl Acad Sci USA* 2016; 113: E3349–58.
- Mori F, Tanji K, Zhang HX, Nishihira Y, Tan CF, Takahashi H, et al. Maturation process of TDP-43-positive neuronal cytoplasmic inclusions in amyotrophic lateral sclerosis with and without dementia. *Acta Neuropathol* 2008; 116: 193–203.
- N'Diaye EN, Kajihara KK, Hsieh I, Morisaki H, Debnath J, Brown EJ. PLIC proteins or ubiquilins regulate autophagy-dependent cell survival during nutrient starvation. *EMBO Rep* 2009; 10: 173–9.
- Nagabhushana A, Bansal M, Swarup G. Optineurin is required for CYLD-dependent inhibition of TNFalpha-induced NF-kappaB activation. *PLoS One* 2011; 6: e17477.
- Nagy N, Farkas K, Kemeny L, Szell M. Phenotype-genotype correlations for clinical variants caused by CYLD mutations. *Eur J Med Genet* 2015; 58: 271–8.
- Neumann M, Sampathu DM, Kwong LK, Truax AC, Micsenyi MC, Chou TT, et al. Ubiquitinated TDP-43 in frontotemporal lobar degeneration and amyotrophic lateral sclerosis. *Science* 2006; 314: 130–3.
- Nicolas A, Kenna KP, Renton AE, Ticozzi N, Faghri F, Chia R, et al. Genome-wide Analyses Identify KIF5A as a Novel ALS Gene. *Neuron* 2018; 97: 1268–83.e6.
- Oakes JA, Davies MC, Collins MO. TBK1: a new player in ALS linking autophagy and neuroinflammation. *Mol Brain* 2017; 10: 5.
- Pilli M, Arko-Mensah J, Ponpuak M, Roberts E, Master S, Mandell MA, et al. TBK-1 promotes autophagy-mediated antimicrobial defense by controlling autophagosome maturation. *Immunity* 2012; 37: 223–34.
- Pottier C, Bieniek KF, Finch N, van de Vorst M, Baker M, Perkersen R, et al. Whole-genome sequencing reveals important role for TBK1 and OPTN mutations in frontotemporal lobar degeneration without motor neuron disease. *Acta Neuropathol* 2015; 130: 77–92.
- Pottier C, Ravenscroft TA, Sanchez-Contreras M, Rademakers R. Genetics of FTL: overview and what else we can expect from genetic studies. *J Neurochem* 2016; 138 (Suppl 1): 32–53.
- Rajan N, Ashworth A. Inherited cylindromas: lessons from a rare tumour. *Lancet Oncol* 2015; 16: e460–e9.
- Rajan N, Langtry JA, Ashworth A, Roberts C, Chapman P, Burn J, et al. Tumor mapping in 2 large multigenerational families with CYLD mutations: implications for disease management and tumor induction. *Arch Dermatol* 2009; 145: 1277–84.
- Ratnavalli E, Brayne C, Dawson K, Hodges JR. The prevalence of frontotemporal dementia. *Neurology* 2002; 58: 1615–21.
- Renton AE, Majounie E, Waite A, Simon-Sanchez J, Rollinson S, Gibbs JR, et al. A hexanucleotide repeat expansion in C9ORF72 is the cause of chromosome 9p21-linked ALS-FTD. *Neuron* 2011; 72: 257–68.
- Ritson GP, Custer SK, Freibaum BD, Guinto JB, Geffel D, Moore J, et al. TDP-43 mediates degeneration in a novel *Drosophila* model of disease caused by mutations in VCP/p97. *J Neurosci* 2010; 30: 7729–39.
- Ruddy DM, Parton MJ, Al-Chalabi A, Lewis CM, Vance C, Smith BN, et al. Two families with familial amyotrophic lateral sclerosis are linked to a novel locus on chromosome 16q. *Am J Hum Genet* 2003; 73: 390–6.
- Seelaar H, Rohrer JD, Pijnenburg YA, Fox NC, van Swieten JC. Clinical, genetic and pathological heterogeneity of frontotemporal dementia: a review. *J Neurol Neurosurg Psychiatry* 2011; 82: 476–86.
- Soo KY, Sultana J, King AE, Atkinson R, Warraich ST, Sundaramoorthy V, et al. ALS-associated mutant FUS inhibits macroautophagy which is restored by overexpression of Rab1. *Cell Death Discov* 2015; 1: 15030.
- Takeuchi H, Kobayashi Y, Yoshihara T, Niwa J, Doyu M, Ohtsuka K, et al. Hsp70 and Hsp40 improve neurite outgrowth and suppress intracytoplasmic aggregate formation in cultured neuronal cells expressing mutant SOD1. *Brain Res* 2002; 949: 11–22.
- Tanaka Y, Nonaka T, Suzuki G, Kametani F, Hasegawa M. Gain-of-function profilin 1 mutations linked to familial amyotrophic lateral sclerosis cause seed-dependent intracellular TDP-43 aggregation. *Hum Mol Genet* 2016; 25: 1420–33.
- Tankard RM, Bennett MF, Degorski P, Delatycki MB, Lockhart PJ, Bahlo M. Detecting tandem repeat expansions in cohorts sequenced with short-read sequencing data. *Am J Hum Genet* 2018; 103: 858–73.
- Teyssou E, Takeda T, Lebon V, Boillee S, Doukoure B, Bataillon G, et al. Mutations in SQSTM1 encoding p62 in amyotrophic lateral sclerosis: genetics and neuropathology. *Acta Neuropathol* 2013; 125: 511–22.
- Thorvaldsdottir H, Robinson JT, Mesirov JP. Integrative Genomics Viewer (IGV): high-performance genomics data visualization and exploration. *Brief Bioinform* 2013; 14: 178–92.
- Tripathi VB, Baskaran P, Shaw CE, Guthrie S. Tar DNA-binding protein-43 (TDP-43) regulates axon growth in vitro and in vivo. *Neurobiol Dis* 2014; 65: 25–34.
- Trompouki E, Hatzivassiliou E, Tschritzis T, Farmer H, Ashworth A, Mosialos G. CYLD is a deubiquitinating enzyme that negatively

- regulates NF-kappaB activation by TNFR family members. *Nature* 2003; 424: 793–6.
- van der Zee J, Gijssels I, Van Mossevelde S, Perrone F, Dillen L, Heeman B, et al. TBK1 mutation spectrum in an extended European patient cohort with frontotemporal dementia and amyotrophic lateral sclerosis. *Hum Mutat* 2017; 38: 297–309.
- Van Mossevelde S, van der Zee J, Gijssels I, Engelborghs S, Sieben A, Van Langenhove T, et al. Clinical features of TBK1 carriers compared with C9orf72, GRN and non-mutation carriers in a Belgian cohort. *Brain* 2016; 139: 452–67.
- Wang K, Li M, Hadley D, Liu R, Glessner J, Grant SF, et al. PennCNV: an integrated hidden Markov model designed for high-resolution copy number variation detection in whole-genome SNP genotyping data. *Genome Res* 2007; 17: 1665–74.
- Wang PY, Chang KT, Lin YM, Kuo TY, Wang GS. Ubiquitination of MBNL1 is required for its cytoplasmic localization and function in promoting neurite outgrowth. *Cell Rep* 2018; 22: 2294–306.
- Watts GD, Wymer J, Kovach MJ, Mehta SG, Mumm S, Darvish D, et al. Inclusion body myopathy associated with Paget disease of bone and frontotemporal dementia is caused by mutant valosin-containing protein. *Nat Genet* 2004; 36: 377–81.
- Webster CP, Smith EF, Bauer CS, Moller A, Hautbergue GM, Ferraiuolo L, et al. The C9orf72 protein interacts with Rab1a and the ULK1 complex to regulate initiation of autophagy. *EMBO J* 2016; 35: 1656–76.
- Wild P, Farhan H, McEwan DG, Wagner S, Rogov VV, Brady NR, et al. Phosphorylation of the autophagy receptor optineurin restricts Salmonella growth. *Science* 2011; 333: 228–33.
- Williams KL, Topp S, Yang S, Smith B, Fifita JA, Warraich ST, et al. CCNF mutations in amyotrophic lateral sclerosis and frontotemporal dementia. *Nat Commun* 2016; 7: 11253.
- Woo JA, Liu T, Trotter C, Fang CC, De Narvaez E, LePochat P, et al. Loss of function CHCHD10 mutations in cytoplasmic TDP-43 accumulation and synaptic integrity. *Nat Commun* 2017; 8: 15558.
- Wu CH, Fallini C, Ticozzi N, Keagle PJ, Sapp PC, Piotrowska K, et al. Mutations in the profilin 1 gene cause familial amyotrophic lateral sclerosis. *Nature* 2012; 488: 499–503.
- Zhang M, Wu X, Lee AJ, Jin W, Chang M, Wright A, et al. Regulation of IkappaB kinase-related kinases and antiviral responses by tumor suppressor CYLD. *J Biol Chem* 2008; 283: 18621–6.